

Non-invasive real-time thermometry via spectral CT physical density quantifications

Nadav Shapira^a, Leening P. Liu^{a,b}, Rizza Pua^a, Derick Rosario^{a,b}, Johoon Kim^{a,b}, David P. Cormode^a, Gregory J. Nadolski^a, Matthew Hung^a, Michael C. Soulen^a, Peter B. Noël^a

^aDepartment of Radiology, University of Pennsylvania, Philadelphia, PA, USA.

^bDepartment of Bioengineering, University of Pennsylvania, Philadelphia, PA, USA

ABSTRACT

Efficient removal of solid focal tumors is a major challenge in modern medicine. Percutaneous thermal ablation is a first-line treatment for patients not fit for surgical resection or when the disease burden is low, mainly due to expedited patient recovery times, lower rates of post-operative morbidity, and reduced healthcare costs. While continuously gaining popularity, ~100,000 yearly thermal hepatic ablation procedures are currently performed without actively monitoring temperature distributions, leading to high rates of incomplete ablations, local recurrences, and damage to surrounding structures. Recent advancements in computed tomography (CT), especially spectral CT, provide promising opportunities for lowering these rates. The additional information available with spectral CT can provide the necessary capabilities to achieve accurate, reliable, on-demand, and non-invasive thermometry during ablation procedures. By taking advantage of our newly developed spectral physical density maps and their direct relation with temperature changes, we performed experiments on phantoms and *ex vivo* tissue to develop, evaluate, optimize, and refine a method for generating thermometry maps from spectral CT scans. Our results validate the accuracy of the spectral physical density model, allowing “whole-organ” mass quantifications that are accurate within one percent, as well as demonstrate an ability to extract temperature changes (linear correlation coefficient of 0.9781) non-invasively and in real-time.

Keywords: Dual-Energy CT, Spectral-CT, Quantitative imaging, Image-guided therapy, Interventional oncology, Tumor ablation, Thermometry.

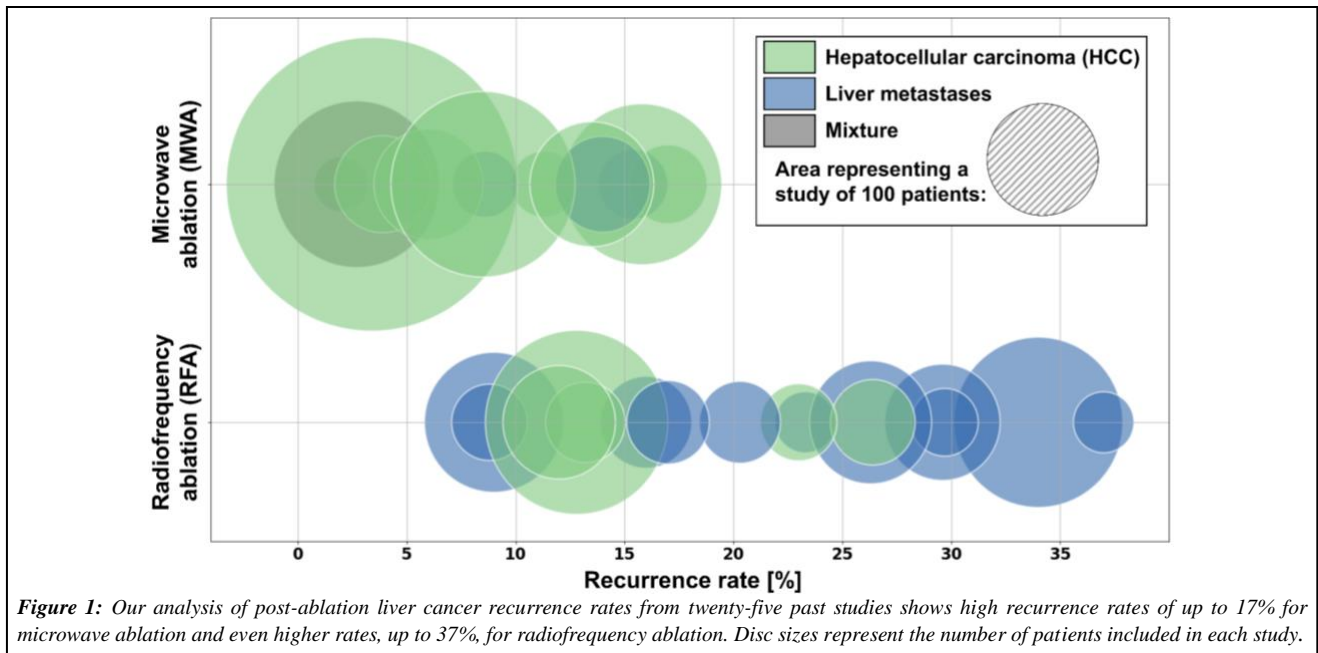
1. INTRODUCTION

With more than 900,000 yearly new cases worldwide, liver cancer is the fifth most common cancer in men and the ninth most common cancer in women¹. Percutaneous thermal ablation techniques provide minimally invasive and inexpensive focal treatment strategies for hepatic tumors^{2,3}. They are considered a first-line treatment for patients with small hepatocellular carcinomas (HCC)⁴, the most common primary malignancy in the liver and the second leading cause of cancer-related mortality in the world⁵, and are used to bridge patients to liver transplantation⁶. Safe and effective ablation treatments rely on complete coverage of the target lesion with lethal temperatures⁷ (≥ 60 °C), while sparing as much surrounding tissue as possible and keeping safety margins to adjacent critical structures⁶. However, despite technological advancements over the past years, local recurrence rates are high (**Figure 1**), burdening patients and healthcare systems.

Published clinical requirements include temperature accuracy of ≤ 2 °C, spatial resolution of ≤ 2 mm, short acquisition, and image generation times for volumetric coverage (≤ 1 minute), metal artifact suppression, and radiation dose levels that meet safety standards⁸. CT-thermometry provides the most promising solution for monitoring thermal ablation treatments. This is mainly because most ablation treatments are already performed under CT guidance, the compatibility of CT with all commercially available ablation systems⁹, and the ability to detect immediate complications, e.g., bleeding. However, despite decades of CT-based thermometry investigations¹⁰, there is a growing demand for solutions to monitor temperatures during ablation procedures.

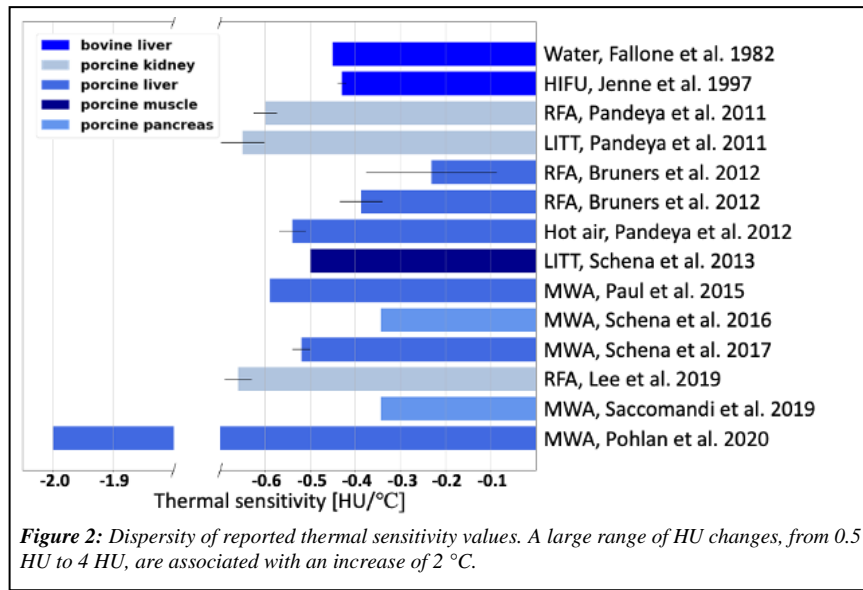
Temperature dependence of CT Hounsfield units (HU) has been observed since the late 1970s¹⁰. Since then, several research groups partially addressed some of the clinical requirements for image-based thermometry listed above with *ex vivo* and *in vivo* experiments. However, several crucial obstacles remain for the anticipated clinical translation of CT-based thermometry.

* e-mail: nadav.shapira@penmedicine.upenn.edu



Temperature assessments from conventional CT rely on attributing shifts in HU to changes in tissue density, which in turn are affected by temperature changes according to thermal volumetric expansion $\rho(T)/\rho_o(T_0) = (1 + \alpha\Delta T)^{-1}$, where $\rho(T)$ is the tissue density at temperature T , ρ_o is the tissue density at a baseline temperature T_0 , ΔT is the change from baseline temperature (in °C), and α is the thermal expansion coefficient associated with the tissue¹⁰. All previous CT-based thermometry studies employed linear or quadratic approximations of the relation above (assuming small ΔT) to correlate temperature and HU changes, which are assumed to be proportional to ρ . While conventional HU depend linearly on tissue density, they are also affected (non-linearly) by changes in tissue composition, which previous studies report as a limiting factor that corrupts temperature accuracy¹⁰. In addition, conventional HU are greatly affected by the scanner model, e.g., tube filtration, and acquisition parameters, e.g., kVp, as well as the patient habitus. This leads to large inconsistencies in thermal sensitivity values seen in previous studies (**Figure 2**). We propose to employ the exact mathematical relationship between tissue density and temperature changes¹⁰, $\Delta T \propto \rho_o(T_0)/\rho(T)$, by utilizing our recently developed spectral physical density quantifications¹¹.

To systematically evaluate our method, we require dedicated phantoms designed to support the development of CT-based solutions for thermometry applications. Tissue-mimicking phantoms that emulate various physical properties of biological tissue are central for the development and evaluation of novel clinical technologies and applications. Compared to *ex vivo* and *in vivo* experiments, phantoms simplify safety, logistical, and cost considerations. For CT-based thermometry applications, phantoms are required to exhibit similar thermal and x-ray to those of human tissue, i.e., thermal conductivity and diffusivity, linear attenuation coefficients within the entire photon energy range relevant to clinical CT imaging. Such phantoms will enable repeatable and controlled experiments that allow rigorous comparisons of temperature sensitivity and reliability on different CT platforms at different imaging protocols.



In this work we report on recent developments aimed for making non-invasive real-time thermometry a reality. We have previously demonstrated accurate physical density quantifications from clinical virtual mono-energetic images (VMI) and effective atomic number (Z_{eff}) spectral results in phantom experiments¹¹. Here we further validate the accuracy of these new spectral maps by utilizing them for non-invasive whole-organ mass estimations on *ex vivo* tissue. While our excellent results attest to the high accuracy of our spectral physical density quantifications, they also present opportunities for novel stand-alone clinical applications. In addition, we demonstrate high correlations between temperature changes and physical density quantifications on *ex vivo* tissue and on thermo-spectral tissue-mimicking phantoms that we developed specifically for this purpose.

2. METHODS

2.1 Thermo-spectral tissue-mimicking phantom development

Our phantoms were developed by iteratively modifying the synthesis method detailed by Negussie and Mikhail *et al.*^{12,13} in order to match the x-ray attenuation curve to that of human liver tissue calculated from well-accepted elemental composition and physical density values¹⁴. These phantoms are particularly useful for thermal therapy experiments since they present comparable thermal properties to those of human tissue. Briefly, 287.5 ml of deionized water in a 1000 ml flask were degassed by purging N_2 for 15 minutes. After degassing, 202.5 ml of 40% (w/v) acrylamide/bis-acrylamide solution was added to the degassed water to achieve 490 ml solution of 16.5% (w/v) acrylamide/bis-acrylamide. While stirring, 6 grams of calcium chloride dissolved in 10 ml of deionized water was added to the acrylamide solution. A single gram of ammonium persulfate in 2 ml of deionized water and a single milliliter of N,N,N',N'-tetramethylethylenediamine were subsequently added to the solution. After stirring for additional 15 seconds, the final solution was immediately transferred to a 475 ml plastic jar.

2.2 Physical density spectral map generation

A complete description of the development of our spectral physical density model, its optimization, and its verification on a tissue characterization phantom (Gammex Model 467, Sun Nuclear) was provided before¹¹. Briefly, 70 keV VMI and Z_{eff} voxel values, which are clinically available on any spectral CT platform, are converted into physical density values through a parametrized Alvarez-Macovski model¹⁵.

2.3 Non-invasive mass measurements

Ex vivo bovine muscle physical density quantifications were evaluated to determine the effect of acquisition parameters on the resulting accuracy. The specimen was weighed with a precision balance (Fisher Scientific Education Precision Balance, Fisher Scientific) to provide ground-truth mass values. Next, the sample was placed on a rectangular block of polyfoam within the 20 cm bore a multi-energy CT phantom (MECT, Sun Nuclear) and scanned with a spectral detector dual-energy CT (IQon spectral scanner, Philips Healthcare) (**Figure 3A**).

Scans were repeated three times at a tube voltage of 120 kVp for each set of collimations {16x0.625, 64x0.625 mm}, dose levels {15.2, 30.3, 45.5 mGy}, and acquisition mode {axial, helical} combinations. No helical scan was acquired with 16x0.625 mm at 45.5 mGy due to tube output limitations. Images were reconstructed with a clinical standard body kernel, a field of view of 350 mm, and at a slice thickness of 2.5 mm with 2.5 mm slice intervals. 70 keV VMIs and Z_{eff} maps were reconstructed from every acquisition and corresponding physical density maps were generated using our spectral physical density model. Regions of interest (ROI) with a diameter of 13.6 mm were positioned in the center of the sample on four consecutive image slices to assess physical density quantification and their dependence on scan parameters. Finally, the sample was weighed after scanning to account for any losses in blood or minor changes in temperature.

To calculate the total mass of the specimen, physical density values were summed from non-air voxels, i.e., 70 keV VMI values larger than -950 HU, and multiplied by the voxel volume ($0.68 \times 0.68 \times 2.5 \text{ mm}^3$). Calculated mass was compared to the average of the two weights, pre- and post-scanning, to evaluate its accuracy with different scanning parameters.

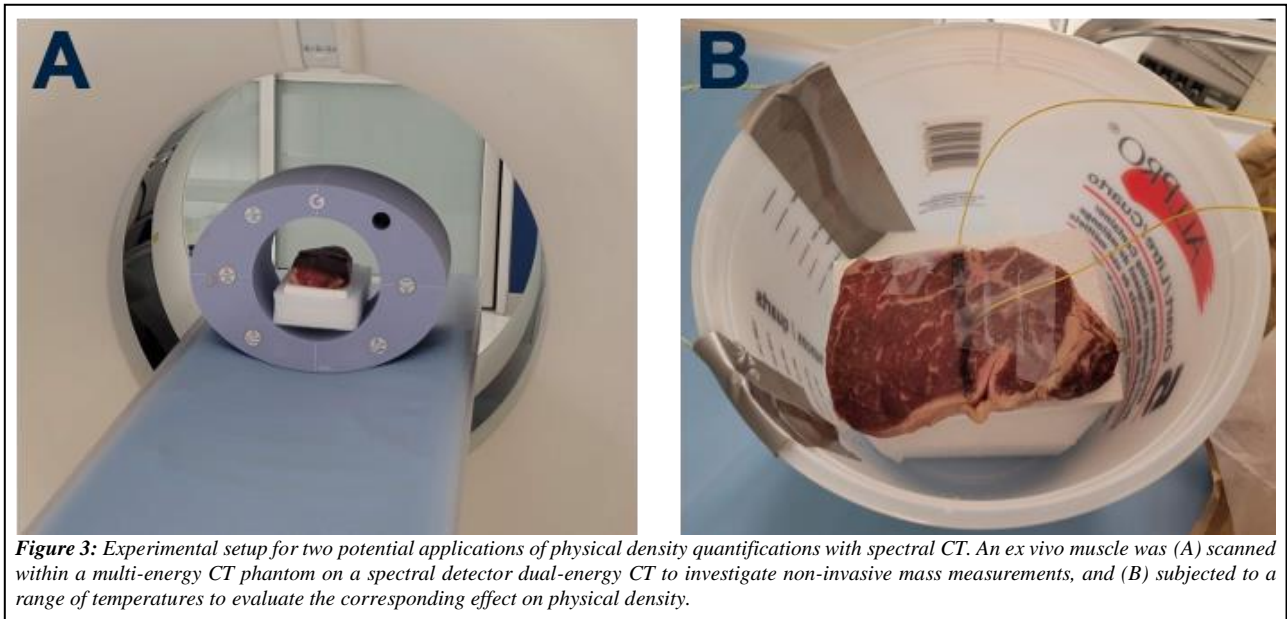


Figure 3: Experimental setup for two potential applications of physical density quantifications with spectral CT. An *ex vivo* muscle was (A) scanned within a multi-energy CT phantom on a spectral detector dual-energy CT to investigate non-invasive mass measurements, and (B) subjected to a range of temperatures to evaluate the corresponding effect on physical density.

2.4 Non-invasive temperature monitoring

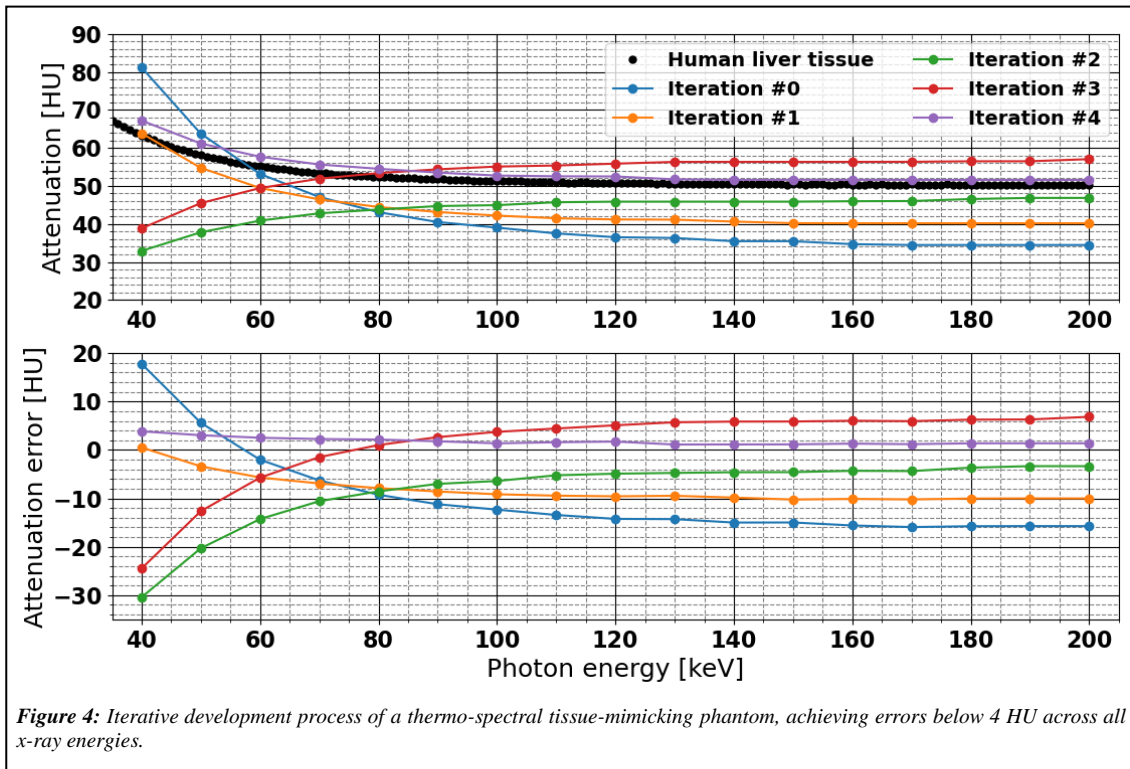
To assess the correlation between changes in temperature and changes in physical density, relative to the physical density values at baseline temperature, optical fiber temperature probes were inserted into the same sample used in the non-invasive mass measurement experiment, as well as three of our dedicated thermo-spectral tissue-mimicking phantoms, using 13-gauge medical trocars to continuously record local internal temperatures (**Figure 3B**). The sample or the phantom was placed in a plastic container, and pre-heated water was poured in to completely submerge it, consequently subjecting it to a wide range of temperatures. After the sample, or phantom, reached an equilibrium temperature, ice was added to cool the water. During heating and cooling, scans were performed approximately every minute with a spectral detector dual-energy CT at a tube voltage 120 kVp, a 16x0.625 mm collimation, a revolution time of 0.75 seconds, and three different radiation dose levels {15.2, 30.3, 45.5 mGy}. For each scan, physical density maps were generated from 70 keV VMI and Z_{eff} spectral results using the same reconstruction parameters detailed in the section above.

The locations of optical fiber temperature probes were determined by thresholding 70 keV VMIs at 90 HU. 4.1 mm diameter ROIs were placed adjacent to the tip of the optical fiber to measure physical density. To elucidate thermal volumetric expansion, physical density values were normalized by dividing the last temporal physical density value with the physical density at a given timepoint. Similarly, the change in temperature was determined relative to the last temporal scan. Linear regressions were fit to the data, where the slopes were associated with the thermal volumetric expansion coefficient. R-values were determined to characterize the correlation between normalized physical density and temperature change.

3. RESULTS

3.1 Thermo-spectral tissue-mimicking phantom development

Attenuation curves that were measured on multiple VMIs, at energies between 40 and 200 keV, with increments of 10 keV, are presented in **Figure 4**. The curves present the iterative developmental process. It enabled us to achieve a maximum error of 4 HU compared to human liver tissue across the entire energy range (Iteration #0 is the scale-down formulation from Negussie and Mikhail *et al.*). Since human livers differ in their elemental compositions, e.g., different fat contents, we deduce that these attenuation errors were sufficiently small for the intended purposes of these phantoms, i.e., the development and testing of spectral CT thermometry approaches.

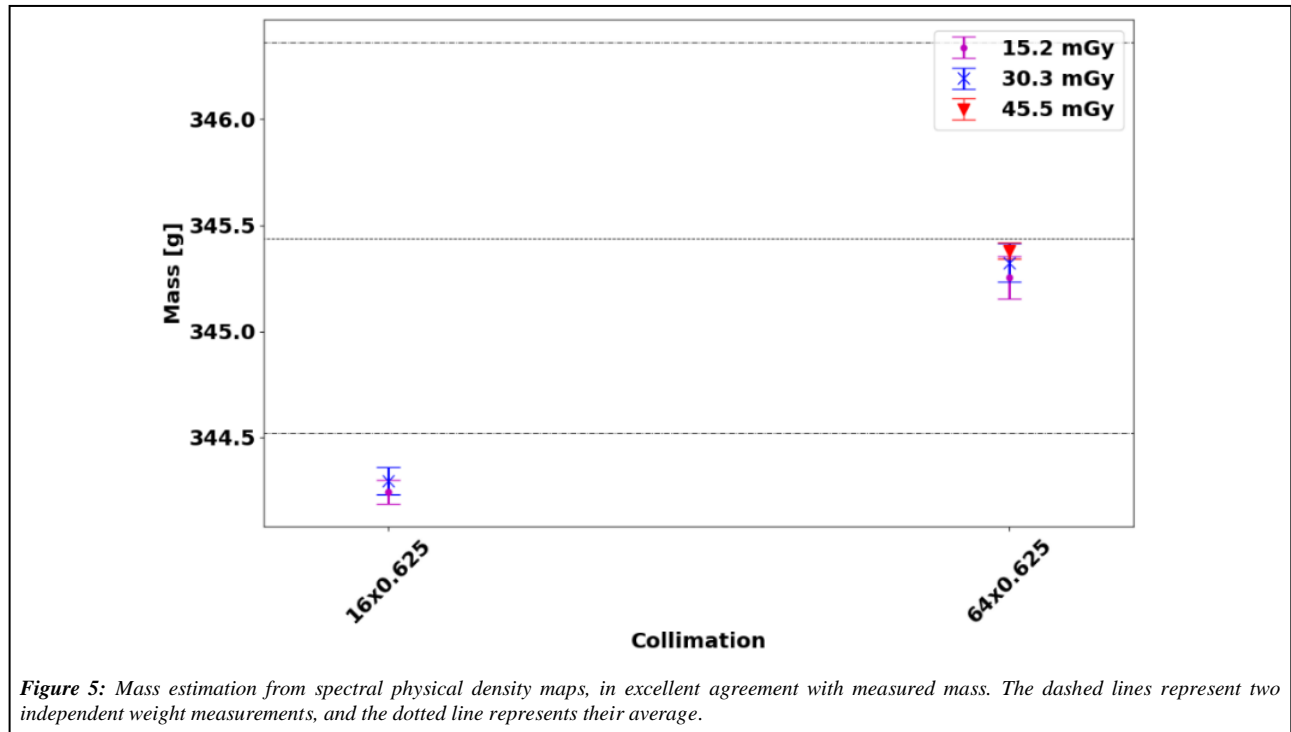


3.2 Non-invasive mass measurements

Spectral physical density quantifications from scans at different doses, collimations, and axial/helical scans revealed that with dose matched scans and different collimations, physical density decreased approximately by 0.003 g/ml with increased collimation. In addition, we observed no effect of dose and axial/helical scans on physical density quantifications.

Non-invasive “whole-organ” mass estimations of the *ex vivo* bovine muscle from scans of varying collimation and dose levels illustrated extremely high accuracies (**Figure 5**). Similar to the physical density quantification, dose levels did not impact the mass value. Between the five different combinations of collimation and dose, estimated mass values were within ± 1.1 grams of ground-truth mass measurements with a scale. For 16x0.625 and 64x0.625 mm collimations, the

errors in mass were -0.34% and -0.04%, respectively. The accuracy of estimated mass further validates our physical density results and demonstrates a clinical application of non-invasive mass measurements for determining the presence of pathology, which is currently utilized only in post-mortem autopsies.



3.3 Non-invasive temperature monitoring

In addition to non-invasive mass measurements, physical density quantifications also enabled non-invasive temperature monitoring as temperature changes are reflected in physical density changes (**Figure 6**). Specifically, a linear fit between normalized physical density and change in temperature demonstrated a slope of $0.00042 \pm 0.00001 \text{ } ^\circ\text{C}^{-1}$ and an intercept of 1.000 ± 0.0003 for temperatures between 22.0 and 45.5 $^\circ\text{C}$. These fit parameters correspond to a 0.42% decrease in physical density with an increase of 10 $^\circ\text{C}$. High linear correlation ($R = 0.9781$) between normalized physical density and change in temperature recapitulated the theoretical relation.

4. CONCLUSION

We have demonstrated the quantitative accuracy of our physical density model on *ex vivo* tissue and on dedicated thermo-spectral phantoms that we have developed specifically for CT-based thermometry applications. In addition, our results demonstrate our ability to employ a well-established and direct relation, i.e., approximation-free, between changes in physical density estimations obtained from spectral CT and changes in temperature. This ability can serve as the backbone of future non-invasive real-time thermometry that is based on non-retrieved spectral information. With the increase in spectral CT utilization and the foreseen replacement of conventional CT scanners by this newer generation systems, we recognize a great opportunity to improve the monitoring and guidance of thermal therapy procedures, which will help reduce the currently high rates of local recurrence.

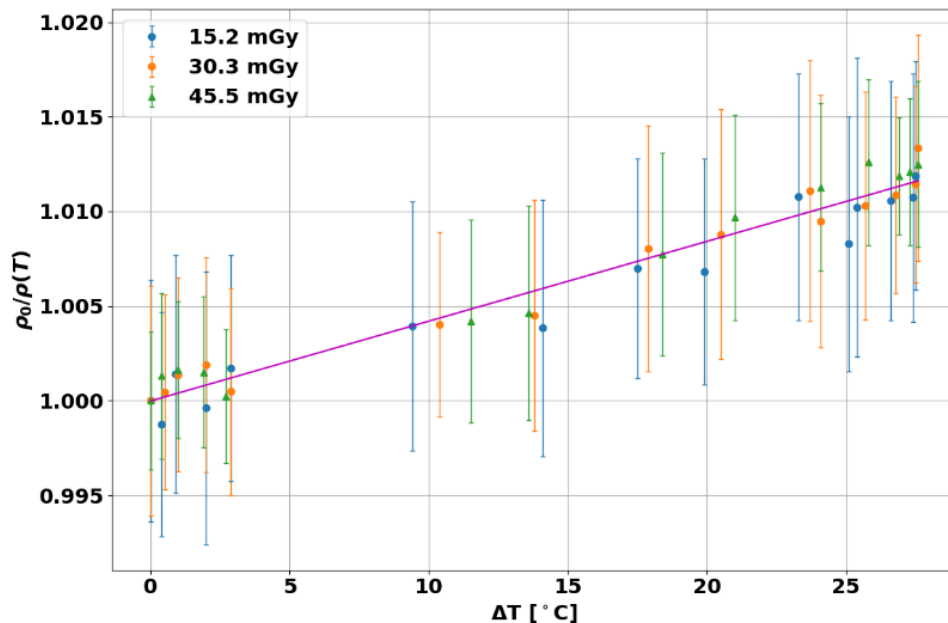


Figure 6: Normalized physical density changes with heating and cooling of ex vivo bovine muscle. The linear relationship between normalized physical density and changes in temperature reflected thermal volumetric expansion.

REFERENCES

1. Liver cancer statistics | World Cancer Research Fund. Available at: <https://www.wcrf.org/dietandcancer/cancer-trends/liver-cancer-statistics>. (Accessed: 24th March 2021)
2. Dodd, G. D., Soulen, M. C., Kane, R. A., Livraghi, T., Lees, W. R., Yamashita, Y., Gillams, A. R., Karahan, O. I. & Rhim, H. Minimally invasive treatment of malignant hepatic tumors: At the threshold of a major breakthrough. *Radiographics* **20**, 9–27 (2000).
3. Froelich, M. F., Schnitzer, M. L., Rathmann, N., Tollens, F., Unterrainer, M., Rennebaum, S., Seidensticker, M., Ricke, J., Rübenthaler, J. & Kunz, W. G. Cost-effectiveness analysis of local ablation and surgery for liver metastases of oligometastatic colorectal cancer. *Cancers (Basel)* **13**, (2021).
4. Izzo, F., Granata, V., Grassi, R., Fusco, R., Palaia, R., Delrio, P., Carrafiello, G., Azoulay, D., Petrillo, A. & Curley, S. A. Radiofrequency Ablation and Microwave Ablation in Liver Tumors: An Update. *The Oncologist* **24**, e990 (2019).
5. McGlynn, K. A., Petrick, J. L. & London, W. T. Global Epidemiology of Hepatocellular Carcinoma: An Emphasis on Demographic and Regional Variability. *Clinics in Liver Disease* **19**, 223–238 (2015).
6. Ringe, K. I., Wacker, F. & Raatschen, H. J. Is there a need for MRI within 24 hours after CT-guided percutaneous thermoablation of the liver? *Acta Radiologica* **56**, 10–17 (2015).
7. Vogl, T. J., Nour-Eldin, N. E. A., Hammerstingl, R. M., Panahi, B. & Naguib, N. N. N. Microwave Ablation (MWA): Basics, Technique and Results in Primary and Metastatic Liver Neoplasms - Review Article. *RoFo Fortschritte auf dem Gebiet der Rontgenstrahlen und der Bildgebenden Verfahren* **189**, 1055–1066 (2017).
8. Frich, L. Non-invasive thermometry for monitoring hepatic radiofrequency ablation. *Minimally Invasive Therapy and Allied Technologies* **15**, 18–25 (2006).
9. Bruners, P., Pandeya, G. D., Levit, E., Roesch, E., Penzkofer, T., Isfort, P., Schmidt, B., Greuter, M. J. W., Oudkerk, M., Schmitz-Rode, T., Kuhl, C. K. & Mahnken, A. H. CT-based temperature monitoring during hepatic RF ablation: Feasibility in an animal model. *International Journal of Hyperthermia* **28**, 55–61 (2012).
10. Fani, F., Schena, E., Saccomandi, P. & Silvestri, S. CT-based thermometry: An overview. *International Journal of Hyperthermia* **30**, 219–227 (2014).

11. Hwang, M., Litt, H. I., Noël, P. B. & Shapira, N. Accurate physical density assessments from clinical spectral results. in *Medical Imaging 2021: Physics of Medical Imaging* (eds. Bosmans, H., Zhao, W. & Yu, L.) **11595**, 45 (SPIE, 2021).
12. Mikhail, A. S., Negussie, A. H., Graham, C., Mathew, M., Wood, B. J. & Partanen, A. Evaluation of a tissue-mimicking thermochromic phantom for radiofrequency ablation. *Medical Physics* **43**, 4304–4311 (2016).
13. Negussie, A. H., Partanen, A., Mikhail, A. S., Xu, S., Abi-Jaoudeh, N., Maruvada, S. & Wood, B. J. Thermochromic tissue-mimicking phantom for optimisation of thermal tumour ablation Thermochromic tissue-mimicking phantom for optimisation of thermal tumour ablation. *International Journal of Hyperthermia* (2016). doi:10.3109/02656736.2016.1145745
14. *Tissue Substitutes in Radiation Dosimetry and Measurement, Report 44 of the International Commission on Radiation Units and Measurements (ICRU)*. (1989).
15. Alvarez, R. E. & Macovski, A. Energy-selective reconstructions in X-ray computerised tomography. *Physics in Medicine and Biology* **21**, 002 (1976).